Sensors & Actuators: B. Chemical 304 (2020) 127413

Contents lists available at ScienceDirect

Sensors and Actuators B: Chemical

journal homepage: www.elsevier.com/locate/snb

Bifunctional pd-decorated polysulfide nanoparticle of Co_9S_8 supported on graphene oxide: A new and efficient label-free immunosensor for amyloid β-protein detection

Yueyuan Li[a], Yaoguang Wang[b], Xuejing Liu[a], Rui Feng[a], Nuo Zhang[a], Dawei Fan[a], Caifeng Ding[c], Huaiqing Zhao[a], Yu Du[a,*], Qin Wei[a,*], Huangxian Ju[a]

[a] Key Laboratory of Interfacial Reaction & Sensing Analysis in Universities of Shandong, School of Chemistry and Chemical Engineering, University of Jinan, Jinan 250022, People's Republic of China
[b] Shandong Provincial Key Laboratory of Molecular Engineering, School of Chemistry and Pharmaceutical Engineering, Qilu University of Technology (Shandong Academy of Sciences), Jinan 250353, People's Republic of China
[c] Key Laboratory of Sensor Analysis of Tumor Marker, Ministry of Education, College of Chemistry and Molecular Engineering, Qingdao University of Science and Technology, Qingdao 266042, People's Republic of China

ARTICLE INFO

Keywords:
G/Co_9S_8-Pd
Dual-functional material
Amyloid β-protein
Immunosensor

ABSTRACT

In this work, bifunctional Pd-decorated Co_9S_8 polysulfide nanoparticles supported on graphene oxide (G/Co_9S_8-Pd) were used to build a label-free immunosensor for amyloid β-protein (Aβ) detection. Grafting Co_9S_8 onto a conductive graphene support can prevent the aggregation of Co_9S_8 and improve the conductivity of the nanocomposites of G/Co_9S_8. A large number of Pd nanoparticles (NPs) were loaded on the G/Co_9S_8 surfaces providing more sites to attach Aβ antibodies by a Pd-N chemical bond. As expected, the novel G/Co_9S_8-Pd nanocomposites with a high specific surface area showed excellent electrocatalytic activity for H_2O_2 reduction and good conductivity. The efficient catalytic activity originated from the synergy between the integrated Co_9S_8, Pd NPs and GO. Additionally, G/Co_9S_8-Pd was applied as a matrix and signal indicator in our immunosensor and obtained a high sensitivity for Aβ detection. The developed immunosensor demonstrated a wide linear range (0.1 pg/mL to 50 ng/mL) and had a low detection limit (41.4 fg/mL). Based on the above, the immunosensor exhibits a remarkable analytical ability and shows potential for a wide range of applications in the field of clinical medical examination and treatment.

1. Introduction

Alzheimer's disease (AD) is a neurodegenerative disease that affects approximately 6 % of the people over the age of 65 [1,2]. Moreover, AD is one of the most expensive diseases in the healthcare industry [3]. Thus, researchers have focused on early diagnose before AD appears. Amyloid β-protein (Aβ) is crucially involved in AD and is neurotoxic. Its deposition in the central nervous system accelerates the progression of AD. Consequently, AD can be confirmed by searching for the Aβ biomarker in cerebrospinal fluid, where the levels of Aβ are lower in AD patients than that in normal controls. Researchers found that Aβ value of AD patients shows a significant reduction of approximately < 500 pg/mL in comparison to 794 ± 20 pg/mL in normal controls [4]. Therefore, an analytical tool is imperatively needed to provide a wide analysis range, rapid detection and high sensitivity for Aβ detection.

Based on the principle of specific binding of antibody and antigen, an immunosensor is a suitable analytical method for Aβ detection [5–7]. This method has the advantages of a wide analytical range, rapid detection and high-sensitivity; furthermore, it has a low cost and does not require large-scale equipment or a large volume during the detection process [8,9]. With these benefits, electrochemical immunosensors have been extensively used in the fields of drug monitoring, food testing, environmental monitoring and disease diagnosis. However, developing efficient and low-cost nanomaterials is imperatively needed in the construction of immunosensors that provide a wide analytical range, rapid detection and high sensitivity for Aβ detection.

In recent years, researchers have focused on novel sensing materials, especially nanomaterials. The developed nanomaterials, such as metal nanoparticles, metal oxides, organics, and metal organic frameworks (MOFs) have been used to fabricate immunosensors for biomarker analytes [10–12]. Among them, some nanoparticles show fast response, good stability and low-cost. Transition metal sulfides have

* Corresponding authors.
E-mail addresses: duyu_ujn@163.com (Y. Du), sdjndxwq@163.com (Q. Wei).

https://doi.org/10.1016/j.snb.2019.127413
Received 24 June 2019; Received in revised form 9 November 2019; Accepted 12 November 2019
Available online 14 November 2019
0925-4005/

attracted the attention of researchers in the nanomaterial field, due to their particular electron structure and rich elements [13,14]. Thus, they have been widely used for electrochemical immunosensors, such as CoS, SnS_2, WS_2 and MoS_2 [15–20]. Among them, a polysulfide compound of cobalt pentlandite (Co_9S_8) has many appealing characteristics due to its unique electronic structure, low cost, good conductivity and high electrocatalytic activities [21,22]. However, the serious agglomeration behavior and low conductivity of Co_9S_8 greatly impedes its usefulness in a wide range of applications. Therefore, grafting Co_9S_8 to a conductive support, such as graphene, is the best way to prevent agglomeration, while improving the conductivity of the nanomaterial [23–25]. Under the above circumstances, an abundance of Co_9S_8 particles are loaded on graphene with a large specific surface area (G/Co_9S_8) because of its highly wrinkled structure. This structure can not only improve the conductivity of the combined material but also improve its electrocatalytic activity toward the H_2O_2 redox reaction. This is due to the good electrocatalytic ability of Co_9S_8 and the synergistic effects between Co_9S_8 and graphene. Furthermore, Co_9S_8 was directly grown on graphene to avoid the use of insulating polymer materials that decreased the number of active sties. As a result, we used Co_9S_8 grafted onto graphene, which was decorated with Pd nanoparticles (G/Co_9S_8-Pd), as a matrix to fabricate an immunosensor for Aβ detection. The introduction of Pd NPs not only further enhanced the electron transfer ability of the matrix and improved the electrocatalytic activity toward the H_2O_2 redox reaction, which significantly enhanced the signal, but also firmly linked antibody (Ab) to the immunosensor by a chemical bond (Pd-N) [26]. As a result, G/Co_9S_8-Pd is a good choice as the matrix and signal indicator of an immunosensor. Under the dual-function of the material, the immunosensor performed well when detecting Aβ.

2. Experimental methods

The preparation process of G/Co_9S_8-Pd and assembly of the immunosensor (Fig. 1) are shown in the supporting information. The fabricated label-free immunosensor was tested using an amperometric *i–t* curve method. First, PBS (10 mL, pH = 7.4) was prepared as base solution. Under a scanned potential of -0.4 V and after a stable background signal was established, 10 μL of H_2O_2 (5 mol/L) was injected into the PBS solution under mild stirring. Finally, the variation of response currents of the tested immunosensor were recorded.

3. Results and discussion

3.1. Characterizations of G/Co_9S_8–Pd

The morphology of GO (Fig. 2A) was observed by scanning electron microscopy (SEM), and a special rippled, flake-like structure was observed. Fig. 2B and C shows the SEM images of G/Co_9S_8. The images showed that small Co_9S_8 nanoparticles were uniformly dispersed on the surface of GO. The formula of Co_9S_8 was determined by EDS (Fig. S1 and Table S1), and the stoichiometry of the polysulfide nanoparticle was verified to be Co: S = 9:8. The Pd NPs were dispersed on the surface of G/Co_9S_8, as displayed by SEM (Fig. 2D) and EDS (Fig. S2) of G/Co_9S_8–Pd. In addition, the crystalline diffraction peaks of G/Co_9S_8 (curve a) and G/Co_9S_8–Pd (curve b) are shown in Fig. 2E. Several prominent diffraction peaks can be found in curve a at 15.4°, 30.9°, 47.1°, and 52.0°, which were assigned to the (111), (311), (511) and (440) crystallographic planes of G/Co_9S_8 (JCPDS no. 65-6801) [27]. The Pd NPs were completely confirmed by the diffraction peak at approximately 40°, in agreement with the standard card of Pd NPs (JCPDS 65–2867) [28]. The results verified that Pd NPs were successfully decorated on the G/Co_9S_8 material.

To further investigate the degree of Co_9S_8 grafted onto GO, X–ray photoelectron spectroscopy (XPS) and transmission electron microscopy (TEM) were carried out. First, the elements of Co, S and C in G/Co_9S_8 were analyzed by XPS (Fig. 2F). The spectrum of Co 2p (Fig. 2G) was divided into six peaks, which can be attributed to Co^{3+} (779.5 eV and 794.4 eV) and Co^{2+} (781.9 eV and 797.8 eV). Furthermore, the peaks at 786.7 eV and 803.6 eV arise from the corresponding satellite peaks (Sat.) of Co^{2+} [29]. As shown in Fig. 2H, the peaks of different binding states from the S spectrum were assigned to C—SC (163.8 eV), CS (164.8 eV), CSO—=—$_2$C (168.7 eV), and CSO—–$_3$C— (169.8 eV) [30]. The results confirmed that the S atoms were successfully incorporated into graphene. As shown in Fig. 2I, the peaks at 284.8 eV and 285.5 eV in the C spectrum were assigned to sp2 graphitic carbon and C—S bonds, respectively. Meanwhile, the peaks at 286.9 eV (C—O-) and 291.4 eV (OCO=—$^-$) were attributed to the efficient thermal elimination of GO [30]. All results showed that Co_9S_8 nanoparticles were successfully grown on GO.

Additionally, G/Co_9S_8 was characterized by TEM, and it was observed that the Co_9S_8 nanoparticles were homogenously distributed throughout the GO (Fig.3A). The high-resolution TEM images (HRTEM,

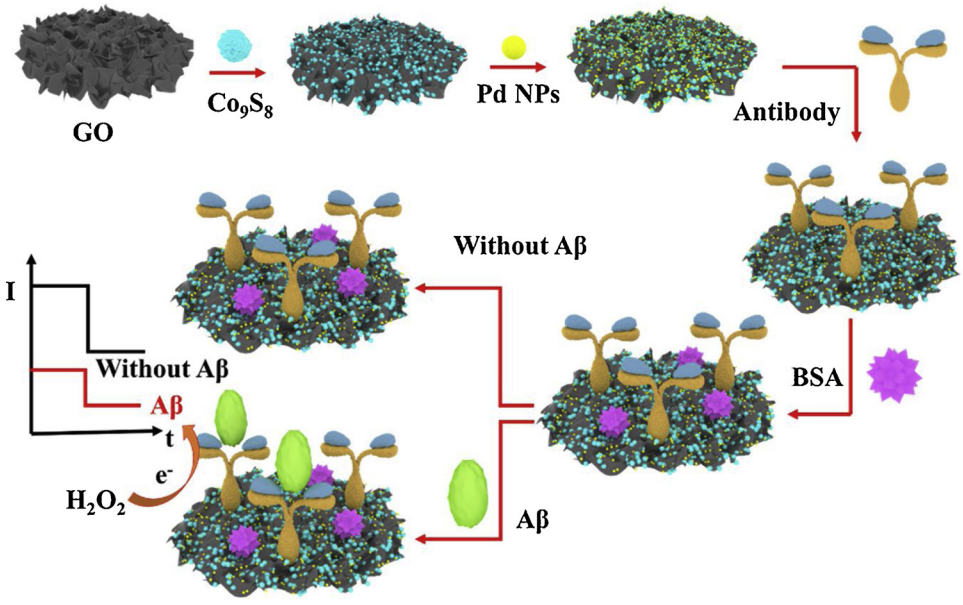

Fig. 1. Schematic presentation of the immunosensor.

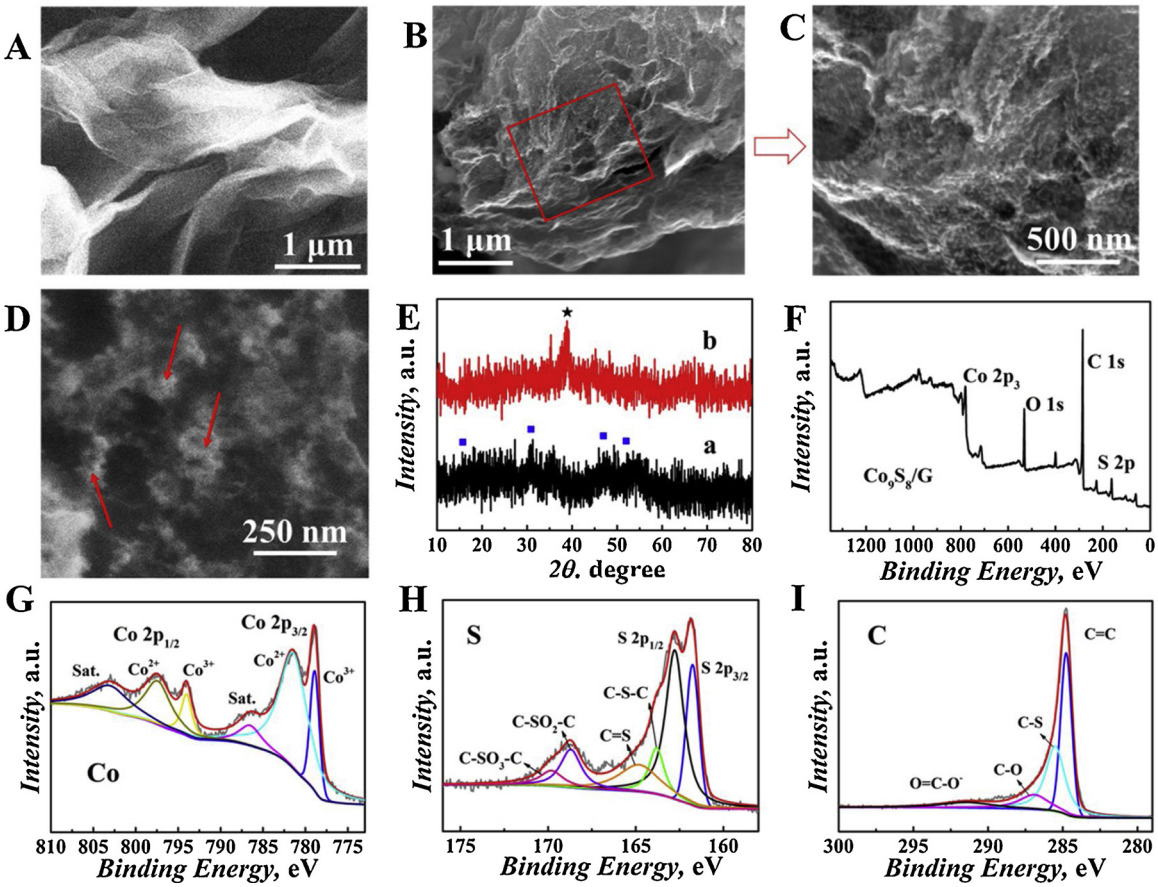

Fig. 2. SEM images of GO (A), G/Co_9S_8 (B and C) and G/Co_9S_8–Pd (D); the XRD plot (E) of G/Co_9S_8 (curve a) and G/Co_9S_8–Pd (curve b); and the XPS spectra of G/Co_9S_8 (F) in the Co (G), S (H) and C (I) regions.

Fig. 3B) of the Co_9S_8 nanoparticles exhibited lattice distances of 0.301 nm and 0.175 nm, corresponding to the (311) and (440) planes, respectively. The graphene nanocrystals were also observed around the Co_9S_8 nanoparticles. In addition, from the TEM image and the corresponding EDS elemental mapping images, it was observed that Co (Fig. 3E) and S (Fig. 3F) elements were distributed homogenously in the GO (C element, Fig. 3D). Thus, the results indicated that the Co_9S_8 nanoparticles were homogenously dispersed in GO.

3.2. Electrochemical characterization

The electrical conductivity (Fig. 4A) and electrocatalytic activity toward the H_2O_2 redox (Fig. S3) of G/Co_9S_8, graphene-Pd and G/Co_9S_8-Pd were characterized. From Fig. 4A, we can observe that the electrical conductivity was improved significantly after the Pd NPs were decorated on the G/Co_9S_8. The electrocatalytic activity ability of G/Co_9S_8-Pd (curve a) was significantly larger than those of G/Co_9S_8 (curve b) or graphene-Pd (curve c). The results verify that G/Co_9S_8-Pd is a good signal indicator for immunosensor.

In addition, electrochemical surface areas (ESA) for the same concentration of GO, G/Co_9S_8 and G/Co_9S_8-Pd (1.0 mg/mL) were tested according to the Cottrell equation written as follows:

$$i_d = \frac{nFAc_o\sqrt{D_o}}{\sqrt{\pi t}}$$

where n is the number of electron transfers ($n = 1$), F is the Faraday constant (F = 96485 C/mol), A is the electrochemical surface area, c_o is the concentration of the electrolyte solution ($c_o = 5 \times 10^{-3}$ mol/L = 5×10^{-6} mol/cm^3), and D_o is the apparent diffusion coefficient of potassium ferricyanide ($K_3Fe(CN)_6$) in 0.1 mol/L KCl solution ($D_o = 0.63 \times 10^{-5}$ cm^2/s). Fig. S4 (A, B and C) shows the detection results of GO, G/Co_9S_8 and G/Co_9S_8-Pd and the red lines in Fig. 4 (B, C and D) represent the straight fitting lines. The $t^{-0.5}$ was an independent variable, and the line slopes were 1.08×10^{-4}, 3.71×10^{-4} and 5.07×10^{-4} ($\frac{A}{\sqrt{s}}$), respectively. 'A' was calculated by the Cottrell equation and the values were 0.158 cm^2, 0.541 cm^2 and 0.742 cm^2 for GO, G/Co_9S_8 and G/Co_9S_8-Pd, respectively. Therefore, the calculated ESA value of G/Co_9S_8 was approximately 3.5 times that of GO. After Pd NPs were decorated on G/Co_9S_8, the detected ESA value become larger, which further confirmed that the G/Co_9S_8-Pd would be a good option as the matrix of the immunosensor. All in all, G/Co_9S_8-Pd is the best choice as the matrix and signal indicator material for fabricating a label free immunosensor.

3.3. Characterization of immunosensor

The EIS Nyquist plots for the modified electrode process are shown in Fig. 5A. As observed in Fig. 5A, bare GCE had a small resistance (curve a). The G/Co_9S_8–Pd modified GCE exhibited a larger resistance (curve b). The resistance gradually increased when Ab (curve c), BSA (curve d) and Aβ (curve e) were modified on the electrode one after another. As a result, the immunosensor was fabricated successfully by a layer by layer method. Subsequently, the fabrication process was monitored by the response current and the results are shown in Fig. 5B. After the modification of Ab (curve b), BSA (curve c) and Aβ (curve d) one after another, the current responses gradually decreased. The results indicated that the immunosensor was fabricated successfully.

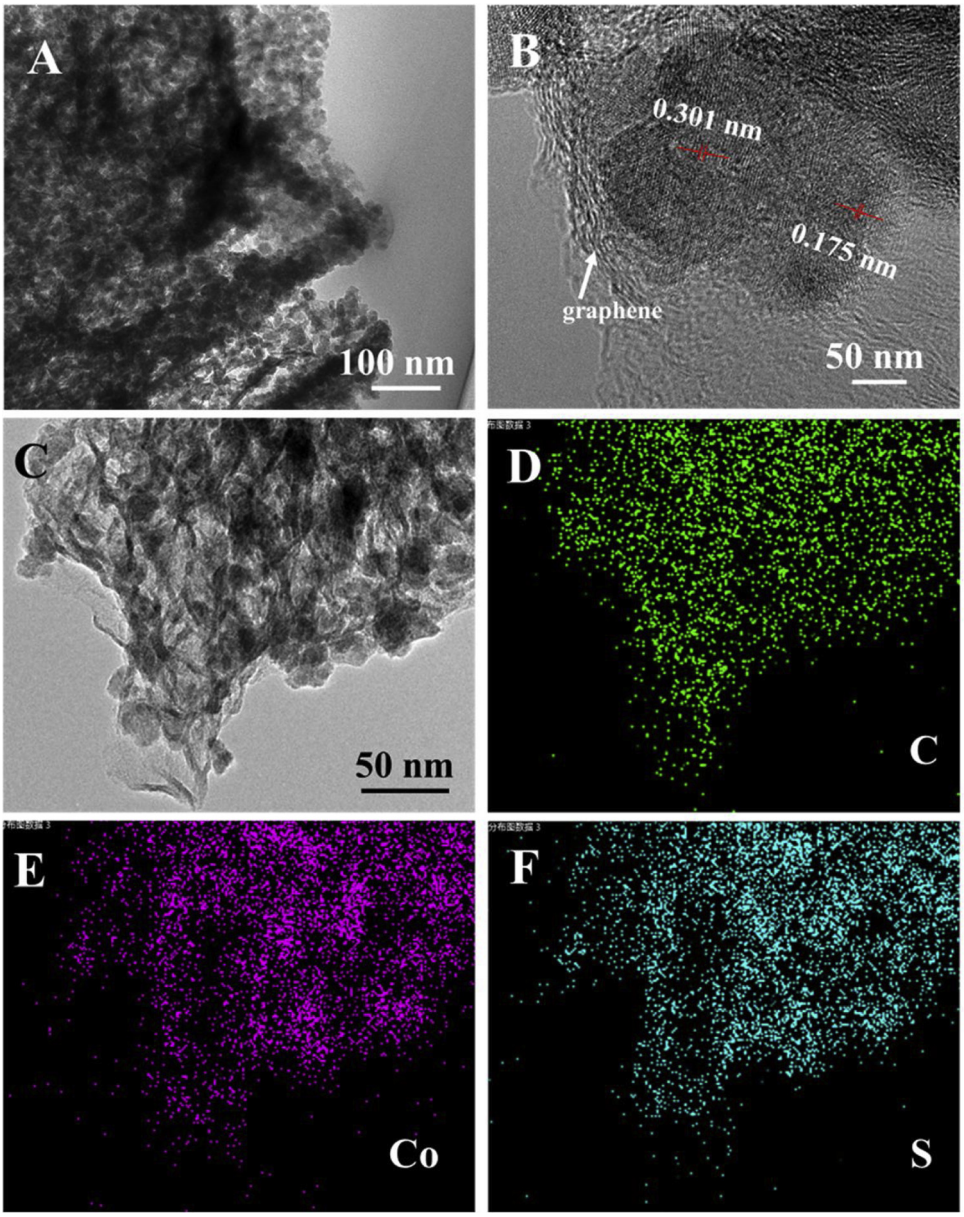

Fig. 3. TEM image (A) and HRTEM image (B) of G/Co_9S_8, and the corresponding EDS elemental mapping images of C (D), Co (E) and S (F) elements in G/Co_9S_8 (C).

3.4. Optimization of the experimental conditions of the immunosensor

The optimal working conditions for the immunosensor were found by testing various pH values and concentrations of G/Co_9S_8–Pd. First, the label-free immunosensor was fabricated by the same concentration of G/Co_9S_8–Pd (1.0 mg/mL) and Aβ (1.0 ng/mL) for finding the optimized pH in the range of 5.3 ~ 8.5. The response currents under different pH values are shown in Fig. 5C. The biggest response current was obtained easily at pH = 7.4. G/Co_9S_8–Pd can not only combine with Ab and promote electron transport, but also generate signals. Thus, the concentration of G/Co_9S_8–Pd was also vital for Aβ detection. The optimal G/Co_9S_8–Pd concentration is shown in Fig. 5D, with a value of 1.0 mg/mL. In short, the optimal experimental conditions for fabricating the G/Co_9S_8–Pd based label-free immunosensor were pH = 7.4 and 1.0 mg/mL of G/Co_9S_8–Pd.

3.5. Analytical performance of the immunosensor

Under the best experimental conditions, the current response increased with increasing Aβ from 0.1 pg/mL to 50 ng/mL (Fig. 6A). The linear regression formula (Fig. 6B) was ΔI (μA) = 115.35–22.54lgc (ng/mL, r = 0.996), and the calculated limit of detection (LOD) was 41.4 fg/mL (Supporting Information) [31]. Compared with those of other reported analytical methods (Table S1), the proposed method showed a comparable result for Aβ detection.

3.6. Selectivity, reproducibility and stability

To assess the selectivity of the proposed immunosensor, a series of interference substances, such as glucose, human immune globulin (HIg), glutamine (Gln) and prostate-specific antigen (PSA), were studied. The detection results in Fig. 6C reveals that the relative standard deviations (RSD) were less than 5.0 %, and there was no significant difference whether it had interference substances. Additionally, reliable reproducibility was also important in the application of the immunosensor. The detected currents of five different electrodes are shown in Fig. 6D, and the RSD was less than 5 %, revealing that the immunosensor presented an acceptable reproducibility. The stability of

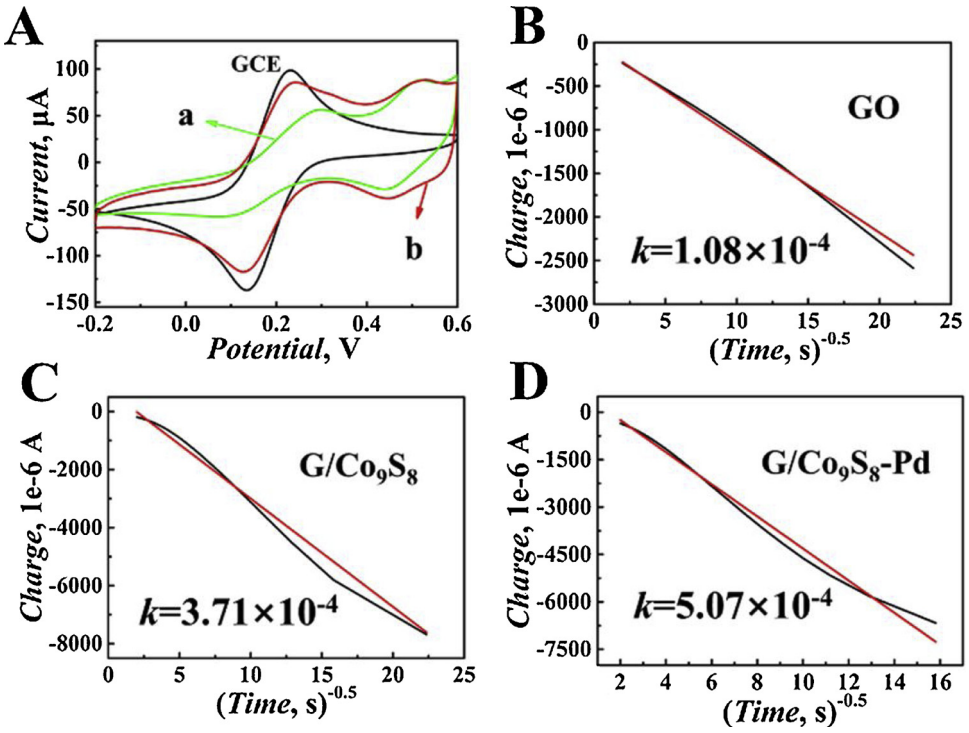

Fig. 4. (A) CV results of G/Co_9S_8 (a) and G/Co_9S_8-Pd (b) in $K_3[Fe(CN)_6]$ (5 mmol/L). The limited current relationships with a -0.5 power of time for GO (B), G/Co_9S_8 (C) and G/Co_9S_8-Pd (D).

the immunosensor was tested for long-term operation. After the fabricated immunosensor was stored at 4 °C for one week, it was found that the response currents showed no significant change. The current decreased 4.1 % when the immunosensor was stored for three weeks. All results demonstrated that the proposed immunosensor exhibited the acceptable selectivity, reproducibility and stability.

3.7. Detection in an artificial cerebrospinal fluid sample

We further investigated the practical application of our immunosensor to detect in a sample of artificial cerebrospinal fluid by using a standard addition recovery experiment. Five different amounts of Aβ (0.005, 0.05, 0.1, 1 and 10 ng/mL) were spiked into an artificial cerebrospinal fluid sample. In Table 1, the recovery of the five samples detection results was in the range of 96.3 % ~109.5 % and the RSD was from 3.9 % to 4.9 %. Hence, the proposed immunosensor would have

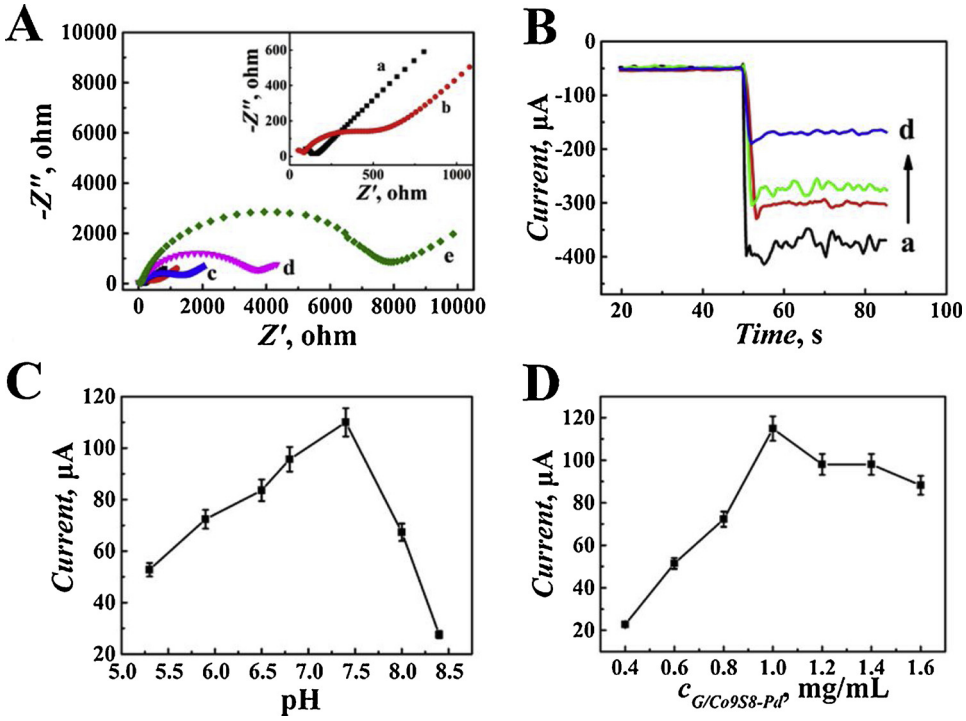

Fig. 5. (A) EIS obtained for the different modified electrodes in $Fe(CN)_6^{3-/4-}$ containing 0.1 mmol/L KCl solution: GCE (a), G/Co_9S_8-Pd/GCE (b), Ab/ G/Co_9S_8-Pd/GCE (c), BSA/Ab/ G/Co_9S_8-Pd/GCE (d) and Aβ/BSA/Ab/ G/Co_9S_8-Pd /GCE (e). (B) The response current of the G/Co_9S_8-Pd/GCE (a), Ab/ G/Co_9S_8-Pd/GCE (b), BSA/Ab/ G/Co_9S_8-Pd/GCE (c) and Aβ/BSA/Ab/ G/Co_9S_8-Pd /GCE (d). The optimization of experimental conditions in reference to the (C) pH and (D) concentration of G/Co_9S_8-Pd on the response of the immunosensor to 1.0 ng/mL Aβ. Error bar = SD (n = 5).

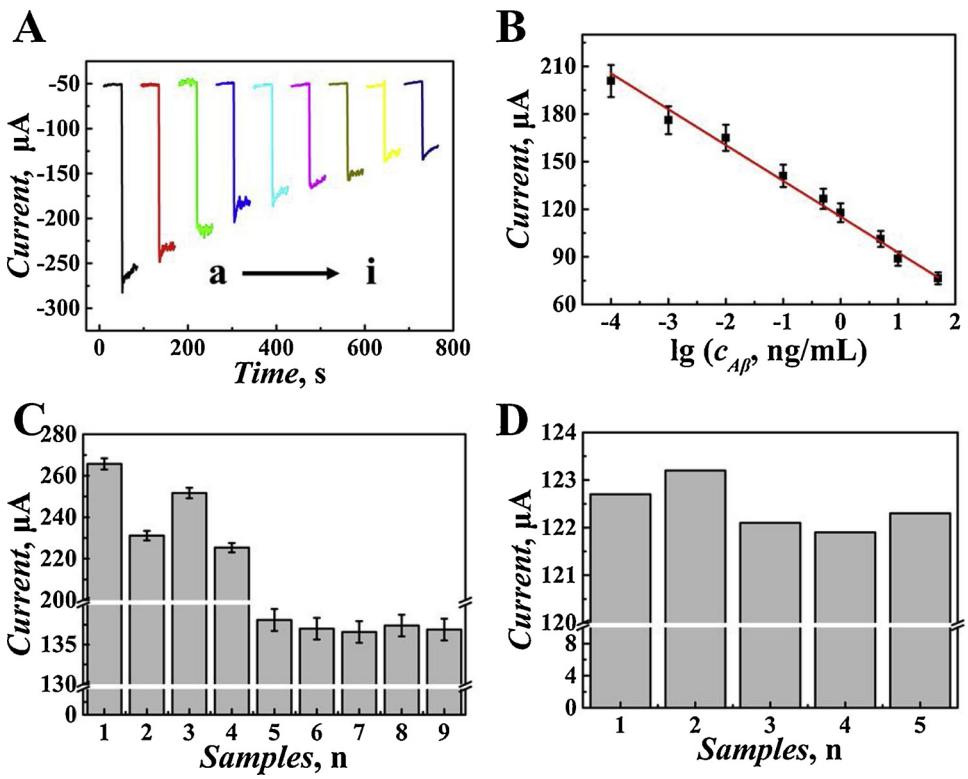

Fig. 6. (A) The current responses of the immunosensor (a ~ k: 0.0001 ng/mL, 0.001 ng/mL, 0.01 ng/mL, 0.1 ng/mL, 0,5 ng/mL, 1 ng/mL, 5 ng/mL, 10 ng/mL and 50 ng/mL). (B) Calibration curve of the immunosensor toward different concentrations of Aβ. (C) The response of the immunosensor to 10 ng/mL glucose (1), 10 ng/mL HIg (2), 10 ng/mL Gln (3), 10 ng/mL PSA (4), 0.1 ng/mL Aβ + 10 ng/mL glucose (5), 0.1 ng/mL Aβ + 10 ng/mL HIg (6), 0.1 ng/mL Aβ + 10 ng/mL Gln (7), 0.1 ng/mL Aβ + 10 ng/mL PSA (8) and 0.1 ng/mL Aβ + 10 ng/mL glucose + 10 ng/mL HIg + 10 ng/mL Gln + 10 ng/mL PSA (9). (D) Current responses of five different electrodes for verifying the reproducibility of the 0.1 ng/mL Aβ modified immunosensor. Error bar = SD (n = 5).

Table 1
The spike recovery test results of the artificial cerebrospinal fluid sample.

Added (ng/mL)	Found (ng/mL)	Average (ng/mL)	RSD (n = 5, %)	Recovery (%)
0.005	0.0056, 0.0051, 0.0050, 0.0054, 0.0052	0.0052	4.7	104.7
0.05	0.054, 0.056, 0.053, 0.058, 0.053	0.055	3.9	109.5
0.1	0.106, 0.104, 0.098, 0.112, 0.101	0.104	4.9	104.1
1	0.93, 1.04, 0.91, 0.97, 0.95	0.96	4.9	96.3
10	9.67, 9.23, 9.59, 10.46, 9.50	9.69	4.8	96.8

great potential for use in a clinical diagnosis of Alzheimer's disease.

4. Conclusion

In this work, a bifunctional G/Co_9S_8-Pd nanocomposite was used to build a label-free immunosensor for Aβ detection. The novel G/Co_9S_8-Pd nanocomposite had good conductivity, high specific surface area and a strong affinity to chemically bond with Ab_1. Thus, G/Co_9S_8-Pd was a good matrix for the fabrication of an immunosensor. Furthermore, the nanocomposite had excellent electrocatalytic activity for H_2O_2 reduction, which was good for enhancing the signal. G/Co_9S_8-Pd was used as the matrix and signal indicator in our immunosensor and obtained a high sensitivity for Aβ detection. The unique G/Co_9S_8–Pd material for fabricating immunosensors is an easy analytical method and a valuable approach for clinical Aβ detection.

Declaration of Competing Interest

The authors declare that they have no known competing financial interests or personal relationships that could have appeared to influence the work reported in this paper.

Acknowledgments

This study was supported by the National Key Scientific Instrument and Equipment Development Project of China (No. 21627809) and the National Natural Science Foundation of China (Nos. 21575050, 21777056). QW thanks the Jinan Scientific Research Leader Workshop Project (2018GXRC024) and UJN. Y.G.W thanks the Program for Scientific Research Innovation Team in the Colleges and Universities of Shandong Province.

Appendix A. Supplementary data

Supplementary material related to this article can be found, in the online version, at doi:https://doi.org/10.1016/j.snb.2019.127413.

References

[1] Alzheimer's disease, BMJ 338 (2009).
[2] J.B. Soriano, A.A. Abajobir, K.H. Abate, S.F. Abera, A. Agrawal, M.B. Ahmed, et al., Global, regional, and national deaths, prevalence, disability-adjusted life years, and years lived with disability for chronic obstructive pulmonary disease and asthma, 1990–2015: a systematic analysis for the Global Burden of Disease Study 2015, Lancet Respir. Med. 5 (2017) 691–706.
[3] C.W. Zhu, M. Sano, Economic considerations in the management of Alzheimer's disease, Clin. Interv. Aging 1 (2006) 143–154.
[4] V. Pérez, L. Sarasa, J.A. Allue, D. Casabona, M. Montanes, D. Insua, et al., Beta-amyloid-17 is a major beta-amyloid fragment isoform in cerebrospinal fluid and blood that shows diagnostic value, Alzheimer Dementia 8 (2012) P240-P.
[5] Y. Wang, G. Zhao, Y. Zhang, B. Du, Q. Wei, Ultrasensitive photoelectrochemical immunosensor based on Cu doped TiO_2 compositing with carbon nitride for detection of carcinoembryonic antigen, Carbon 146 (2019) 276–283.
[6] Q. Yan, L.L. Cao, H. Dong, Z.L. Tan, Y.T. Hu, Q. Liu, et al., Label-free immunosensors based on a novel multi-amplification signal strategy of TiO_2-NGO/Au@Pd hetero-nanostructures, Biosens. Bioelectron. 127 (2019) 174–180.
[7] L. Liu, Y. Chang, J. Yu, M.S. Jiang, N. Xia, Two-in-one polydopamine nanospheres for fluorescent determination of beta-amyloid oligomers and inhibition of beta-amyloid aggregation, Sens. Actuators B Chem. 251 (2017) 359–365.
[8] F. Ricci, G. Adornetto, G.J.E.A. Palleschi, A review of experimental aspects of electrochemical immunosensors, Electrochim. Acta 84 (2012) 74–83.
[9] X.L. Liang, N. Bao, X.L. Luo, S.N. Ding, CdZnTeS quantum dots based electrochemiluminescent image immunoanalysis, Biosens. Bioelectron. 117 (2018) 145–152.
[10] L. Liu, D.H. Deng, W.F. Sun, X.H. Yang, S.L. Yang, S.J. He, Electrochemical biosensors with electrocatalysts based on metallic nanomaterials as signal labels, Int. J. Electrochem. Sci. 13 (2018) 10496–10513.
[11] M. Tang, Z.X. Zhou, S.G. Li, F. Zhao, S.Q. Liu, Electrochemiluminescent detection of

cardiac troponin I by using soybean peroxidase labeled-antibody as signal amplifier, Talanta 180 (2018) 47–53.
[12] W.J. Jiang, H.S. Yin, Y.L. Zhou, J.L. Duan, H.S. Li, M.H. Wang, et al., A novel electrochemiluminescence biosensor for the detection of 5-methylcytosine, TET 1 protein and beta-glucosyltransferase activities based on gold nanoclusters-H_2O_2 system, Sens. Actuators B Chem. 274 (2018) 144–151.
[13] M.J. Choi, J. Kim, J.K. Yoo, S. Yim, J. Jeon, Y.S. Jung, Extremely small pyrrhotite Fe_7S_8 nanocrystals with simultaneous carbon-encapsulation for high-performance Na-Ion batteries, Small 14 (2018) 6.
[14] X. Deng, K. Li, X. Cai, B. Liu, Y. Wei, K. Deng, et al., A hollow-structured CuS@Cu_2S@Au nanohybrid: synergistically enhanced photothermal efficiency and photoswitchable targeting effect for Cancer theranostics, Adv. Mater. 29 (2017).
[15] C.J. Sui, T.T. Wang, Y.L. Zhou, H.S. Yin, X.J. Meng, S.R. Zhang, et al., Photoelectrochemical biosensor for hydroxymethylated DNA detection and T4-beta-glucosyltransferase activity assay based on WS_2 nanosheets and carbon dots, Biosens. Bioelectron. 127 (2019) 38–44.
[16] F.B. Pei, P. Wang, E.H. Ma, Q.S. Yang, H.X. Yu, J. Liu, et al., A sensitive label-free immunosensor for alpha fetoprotein detection using platinum nanodendrites loaded on functional MoS_2 hybridized polypyrrole nanotubes as signal amplifier, J. Electroanal. Chem. Lausanne (Lausanne) 835 (2019) 197–204.
[17] Y.G. Wang, D.W. Fan, G.H. Zhao, J.H. Feng, D. Wei, N. Zhang, et al., Ultrasensitive photoelectrochemical immunosensor for the detection of amyloid beta-protein based on SnO_2/SnS_2/Ag_2S nanocomposites, Biosens. Bioelectron. 120 (2018) 1–7.
[18] A.R. Liu, H.T. Shan, M.Y. Ma, S.G. Li, K.P. Jiang, M.K. Shi, et al., An ultrasensitive photoelectrochemical immunosensor by integration of nanobody, TiO_2 nanorod arrays and ZnS nanoparticles for the detection of tumor necrosis factor-alpha, J. Electroanal. Chem. Lausanne (Lausanne) 803 (2017) 1–10.
[19] Y.L. Zhou, H.S. Yin, Y. Wang, C.J. Sui, M.H. Wang, S.Y. Ai, Electrochemical aptasensors for zeatin detection based on MoS_2 nanosheets and enzymatic signal amplification, Analyst 143 (2018) 5185–5190.
[20] Y. Li, W. Zhu, Q. Kang, L. Yang, Y. Zhang, Y. Wang, et al., Dual-mode electrochemical immunoassay for insulin based on Cu_7S_4–Au as a double signal Indicator, ACS Appl. Mater. Interfaces 10 (2018) 38791–38798.
[21] Y. Gao, L. Kang, Y. Lian, W. Xin, R. Wang, J. Liang, et al., In-situ sulfuration synthesis of N,S-doped carbon nanosheet encapsulated Fe-doped Co_9S_8 as anodes for tunable lithium storage, Appl. Surf. Sci. 473 (2019) 673–680.
[22] L. Li, Y. Ding, H. Huang, D. Yu, S. Zhang, H.-Y. Chen, et al., Controlled synthesis of unique Co_9S_8 nanostructures with carbon coating as advanced electrode for solid-state asymmetric supercapacitors, J. Colloid Interface Sci. 540 (2019) 389–397.
[23] J. Kusuma, R.G. Balakrishna, S. Patil, M.S. Jyothi, H.R. Chandan, R. Shwetharani, Exploration of graphene oxide nanoribbons as excellent electron conducting network for third generation solar cells, Sol. Energy Mater. Sol. Cells 183 (2018) 211–219.
[24] L. Liu, K. Zheng, Y. Yan, Z. Cai, S. Lin, X. Hu, Graphene aerogels enhanced phase change materials prepared by one-pot method with high thermal conductivity and large latent energy storage, Sol. Energy Mater. Sol. Cells 185 (2018) 487–493.
[25] X. Liu, T. Xu, Y. Li, Z. Zang, X. Peng, H. Wei, et al., Enhanced X-ray photon response in solution-synthesized $CsPbBr_3$ nanoparticles wrapped by reduced graphene oxide, Sol. Energy Mater. Sol. Cells 187 (2018) 249–254.
[26] Z. Wei, Z. Hai, M.K. Akbari, Z. Zhao, Y. Sun, L. Hyde, et al., Surface functionalization of wafer-scale two-dimensional WO_3 nanofilms by NM electrodeposition (NM = Ag, Pt, Pd) for electrochemical H_2O_2 reduction improvement, Electrochim. Acta 297 (2019) 417–426.
[27] Q. Wei, B. Baoguo, B. Di, G. Peng, The preparation of Co_9S_8 and CoS_2 nanoparticles by a high energy ball-milling method and their electrochemical hydrogen storage properties, Int. J. Hydrogen Energy 39 (2014) 9300–9306.
[28] J.M.M. Tengco, Y.K. Lugo-José, J.R. Monnier, J.R.J.C.T. Regalbuto, Chemisorption–XRD particle size discrepancy of carbon supported palladium: carbon decoration of Pd? Catal. Today 246 (2015) 9–14.
[29] Y. Wei, X. Ren, H. Ma, X. Sun, Y. Zhang, X. Kuang, et al., $CoC_2O_4{\cdot}2H_2O$ derived Co_3O_4 nanorods array: a high-efficiency 1D electrocatalyst for alkaline oxygen evolution reaction, Chem. Commun. 54 (2018) 1533–1536.
[30] Y. Tang, F. Jing, Z. Xu, F. Zhang, Y. Mai, D. Wu, Highly crumpled hybrids of nitrogen/sulfur dual-doped graphene and $Co9S_8$ nanoplates as efficient bifunctional oxygen electrocatalysts, ACS Appl. Mater. Interfaces 9 (2017) 12340–12347.
[31] IUPAC, nomenclature, symbols, units and their usage in Spectrochemical analysis - II. Data interpretation, Pure Appl. Chem. 33 (2008) 241–245.

Yueyuan Li is a current Ph. D. student, studies in School of Chemistry and Chemical Engineering, University of Jinan. She is working on constructing electrochemical sensor.

Yaoguang Wang received his B.S. degree in chemistry from University of Jinan in 2012, M.S. degree in chemical engineering and technology from University of Jinan in 2015 and Ph.D. degree in chemical engineering and technology from University of Jinan in 2019. Now, he is an associate professor in Qilu University of Technology (Shandong Academy of Sciences). His main research interests are electrochemical sensors and biosensors.

Xuejing Liu received her Ph.D. degree in College of Chemistry from Dalian University of Technology in 2015. From 2015–2018, she worked as a postdoctoral fellow in Dalian Institute of Chemical Physics. At present, she begins to work in School of Chemistry and Chemical Engineering from University of Jinan. Her main interest is in the theoretical investigation of catalyst materials for applications in small molecules activation and conversion, electrocatalytic of water splitting, reduction of CO2 and N2, etc.

Rui Feng received her PhD degree at Research Center for Eco-environmental Science, Chinese Academy of Sciences, and University of the Chinese Academy of Sciences in 2018. Now, she is a lecturer at University of Jinan. Her current research interests: construction of electrochemical sensor and its application in environmental testing.

Nuo Zhang received her B.S. degree in biological technology from University of Jinan in 2007 and M.S. degree in analytical chemistry from University of Jinan in 2010. Now, she is a lecturer at University of Jinan. Her main research interests are electrochemical biosensors and photoelectrochemical biosensors.

Dawei Fan got her Ph. D. from Lanzhou Institute of Chemical Physics, Chinese Academy of Sciences. Her main research interests are the construction of orderly self-assembled structures, research of photochemical and electrochemical sensors. He has published over 30 research papers including Angew. Chem. Int. Edit., Biosens. Bioelectron., J. Phys. Chem. C, Amino Acids, J. Colloid. Interf. Sci., Phys. Chem. Chem. Phys., Talanta.

Caifeng Ding joined College of Chemistry and Molecular Engineering, Qingdao University of Science and Technology.

Huaiqing Zhao joined School of Chemistry and Chemical Engineering from University of Jinan.

Yu Du joined School of Chemistry and Chemical Engineering from University of Jinan.

Qin Wei a professor and DSc, has devoted herself to analytical teaching and scientific research. Her main research interests are the determination of protein and nucleic acid by photometry and the electrochemical immunosensor preparation. She has published over one hundred articles on analysis, immunosensor and applied successfully for many research projects, such as Biomaterials, Adv. Mater., Adv. Funct. Mater., Anal. Chem., Biosens. Bioelectron., Sens. Actuators B: Chem., Talanta.

Huangxian Ju received his BS, MS and Ph.D. degrees from Nanjing University during 1982–1992. He was a postdoc in Montreal University (Canada) from 1996 to 1997 and a guest professor in three universities of Germany and Ireland in 1999-2000. He became an associate and full professor of Nanjing University in 1993 and 1999. He is currently the director of State Key Laboratory of Analytical Chemistry for Life Science. His research interests focus on analytical biochemistry, biosensing and molecular diagnosis. He has published 616 papers in different journals with SCI h-index of 83 (29,523 citations) and Google Scholar h-index of 91 with more than 29000 citations.